RSC Advances

Hydrodeoxygenation of phenol as a bio-oil model compound on intimate contact

noble metal-Ni$_2$P/SiO$_2$ catalyst

Yunhua Li[*], Xin Yang, Linhui Zhu, Hua Zhang, Binghui Chen

Department of Chemical and Biochemical Engineering, College of Chemistry and Chemical Engineering, National Engineering

Laboratory for Green Chemical Productions of Alcohols-Ethers-Esters, Xiamen University, Xiamen 361005, PR China.

Abstract: This study investigates phenol hydrodeoxygenation on supported Ni$_2$P from the sol-gel and TPR

method and noble metal (Pd, Pt and Ru)-Ni$_2$P catalysts from Ni$_2$P partially in-situ reducing noble metal precursor.

10%Ni$_2$P/SiO$_2$ had the relatively uniform distribution of Ni$_2$P nanoparticle and high active activity for phenol

hydrodeoxygenation. Phenol conversion increased with the increasing in reaction temperature and the main

products on noble metal-Ni$_2$P/SiO$_2$ also changed from cyclohexanol at 453K to cyclohexane at 493K. In

comparison with supported Ni$_2$P or noble metal catalysts and their physical mixture, Pd-Ni$_2$P/SiO$_2$ presented the

highest conversion activity and cyclohexane selectivity. Physiochemical characterizations showed that the active

sites over catalysts increased and electron transferring occurred from Ni$_2$P to noble metal due to intimate contact

between Ni$_2$P and noble metal. Synergistic effect of deoxygenation and carbonyl hydrogenation from Ni$_2$P and

hydrodeoxygenation from Pd resulted in improvement of catalytic activity and differences of selectivity on

catalysts.

Keywords: Hydrodeoxygenation, Phenol, Bio-oil, Nickel phosphide, Noble metal

1. Introduction

Most effort has focused on production of renewable and clear biofuels and chemicals due to energy consumption

---

* Corresponding author. E-mail: yunhuali@xmu.edu.cn.

and environmental deterioration. Lignin, typically composed of methoxy-substituted phenyl propanoid units, is the second most abundant component in biomass and can be regarded as a potential resource for the production of biofuels and special chemicals [1]. Bio-oil from lignin, however, cannot be used without prior refining due to its high viscosity, low heating value and corrosiveness. Thus, hydrodeoxygenation (HDO) has been developed to convert this biofuel with these undesirable properties into feasible vehicle fuel.

Up to now, hydrodeoxygenation catalysts mainly include the traditional MoS_2, noble metal and transition metal phosphide based catalysts [2-4]. Among them, nickel phosphide has been prepared from the traditional temperature programmed reduction (TPR) method. However, there are still problems such as high preparation temperature and the lager and uncontrollable particle size of nickel phosphide in this method. For this reason, several other processes have been developed, such as the solution-phase method [5], the decomposition of metal hypophosphites [6] and converting metal nanoparticles into metal phosphides [7].

At the same time, a series of composite catalysts for hydrodeoxygenation of guaiacol or phenol, the common model chemicals in biofuel, have also been studied [8, 9]. For example, Yan et al. [10] catalyzed hydrodeoxygenation of phenols using Ru nanoparticle catalysts combined with brønsted acidic ionic liquids. Hong et al. [11] prepared Pd/WOx/γ-Al$_2$O$_3$ for guaiacol hydrodeoxygenation. With respect to bimetallic catalysts containing transition metal phosphide, Pd-Ni$_2$P/C has presented 1.5 times higher power density than commercial Pd for direct formic acid fuel cells [12]. Ni$_2$P could also enhance the activity and durability of the Pt anode catalyst in direct methanol fuel cells [13]. In addition, some researchers also noticed that programmed reduction temperature for phosphate decreased and the hydrodesulfurization activity increased with the addition of Pd or Pt into Ni$_2$P supported catalyst [14]. However, these catalysts have usually been obtained by impregnating passivated phosphide or phosphate with noble metal precursor solution. It is difficult to ensure the directional loading of noble metal and the formation of intimate contact between phosphide and noble metal due to nonselective deposition of noble metal on support or phosphate.

It is noteworthy that transition metal phosphide requires further passivation to avoid the drastic oxidation of nickel phosphide when it is exposure to air. This means that phosphide has certain reducibility.

Herein, supported nickel phosphide was firstly prepared from the sol-gel and the traditional TPR method. Thus, Ni_2P was uniformly dispersed over SiO_2. The as-prepared supported nickel phosphide was then impregnated by noble metal precursor solution to obtain noble metal-Ni_2P catalyst. This preparation process not only favors the distribution of noble metal and minimizes its usage due to controllable distribution of reductant Ni_2P, but also facilitates the formation of intimate contact structure and intensifies the interaction between noble metal and Ni_2P. The catalytic HDO evaluation and catalyst characterizations were conducted on supported Ni_2P, noble metal and noble metal-Ni_2P catalysts. Results showed that noble metal-Ni_2P/SiO_2 has the higher catalytic performances for phenol hydrodeoxygenation due to the more active site and electron transfer from Ni_2P to Pd than supported Ni_2P or noble metal catalysts. Based on these outcomes, relations between structure and catalytic performance were also discussed. The result may provide valuable information for developing Ni_2P or noble metal based catalyst to upgrade bio-crude-oil to feasible fuel.

2. Experimental

2.1. General

Chemical reagents (GC grade) used for analysis, such as benzene, phenol, cyclohexanol, cyclohexane, cyclohexene, cyclohexanone, isooctane, docecane and noble metal precursors were from Aladdin Chemistry Co., Ltd. All other chemicals were of analytical grade from sinopharm chemical reagent Co.,Ltd and were used as received without any further purification.

2.2. Preparation of Ni_2P/SiO_2 catalysts and noble metal-Ni_2P/SiO_2

Ni_2P/SiO_2 was prepared via a sol-gel process according to the reference [7]. In the typical preparation, a

homogeneous solution of 2.62 g $Ni(NO_3)_2 \cdot 6H_2O$, 4.2 g urea and 225 ml H_2O was kept in a conical flask at 303 K,

and its pH value was adjusted at 2.5 using diluted HNO_3 solution. A solution of 22.4 ml tetraethyl orthosilicate

(TEOS) and 20 ml ethanol was dropwise added to the above solution under the stirring. The as-prepared sample

was then heated to 363 K, filtered at pH 8.0, dried at 393K for 12h and calcined in U-tube quartz reactor at 823K

for 5h to obtain Ni/SiO_2. Ni_2P/SiO_2 was further prepared from the traditional TPR method using $NH_4H_2PO_4$

solution impregnating the as-prepared Ni/SiO_2 sample. The nominal Ni/P ratio of the catalyst was 1.0. After

impregnation for 12h, the sample was calcined at 823K in air atmosphere for 4h. After cooled to room temperature,

the sample was reduced at 923K in a H_2 flow for 3h and passivated under 1.5% O_2/N_2 for 6h at room temperature.

The noble metal-Ni_2P/SiO_2 was prepared by in-situ reduction of noble metal precursors. The detailed

procedure is as follows. After the preparation of fresh Ni_2P/SiO_2 in U-tube quartz reactor was completed, a H_2 flow

was switched into a N_2 atmosphere. This reactor filled with N_2 was placed in the ultrasonic cleaner (KQ-250DE).

A certain concentration of noble metal precursor, such as $PdCl_2$, H_2PtCl_6, $RuCl_3$, solution was injected with a

syringe into the freshly prepared Ni_2P/SiO_2 in U-tube quartz reactor under the ultrasound condition. The

concentration of noble metal precursor was 0.01g/mL and corresponding liquid volume used is based on the

nominal loading of noble metal, 1%. After 40min, the sample was washed, dried under H_2 at 393K for 2h and

passivated under 1.5% O_2/N_2 for 3h.

For comparison, supported pure noble metal catalysts were prepared from impregnation method. The

preparation of support SiO_2 was similar to that of Ni/SiO_2 except on addition of nickel precursor. After

impregnating noble metal precursor solution for 12h, the samples were calcined under H_2 at 723K for 3h.

2.3. Physiochemical Characterization

The X-ray powder diffraction (XRD) measurements were carried out on a PAN-alytical X-ray diffractometer

with Cu Ka ($\lambda = 0.15406$ nm) radiation. A continuous scan mode was used to collect 2θ data from 10° to 90° with a

step width of 0.0167°. Transmission electron microscopy (TEM) images were collected using a JEOL JEM-1400

instrument. The samples were prepared by dispersing the powders in ethanol and then dropping a small volume

onto a carbon-coated copper grid.

Specific surface area was determined by N_2 adsorption-desorption isotherms method at 77K using a

Micrometrics ASAP 2020 system and calculated by the BET (Brunauer–Emmett–Teller) method. The pore

structure parameters were calculated from BJH (Barrett-Joiner-Halenda) method. Prior to the analysis, the samples

were outgassed at 523 K for 3h to eliminate volatile adsorbates on the surface.

CO chemisorption was performed (Micromeritics ASAP 2020) to provide an estimate of the active sites on

the samples. Usually, 0.1 g passivated sample was loaded into a quartz reactor and re-reduced in a H_2 flow (40

mL/min) at 723 K for 2 h. After evacuated for 1 h at this temperature, the samples were cooled down to RT in a He

(60 mL/min). Subsequently the first isotherm was taken. After the first isotherm was measured, the sample was

evacuated for 2 h. The second isotherm was performed. The CO chemisorption obtained was calculated by

subtracting amounts of adsorbed CO with the second isotherms.

To characterize the structure and composition of the catalysts, the high angle annular dark field scanning

transmission electron microscopy (HAADF-STEM) and energy-dispersive X-ray spectroscopy (EDS) were

performed on a FEI TECNAI F30. X-ray photoelectron spectroscopy (XPS) measurements were performed using a

Quantum 2000 Scanning ESCA Microprobe system with Al Kα radiation under ultrahigh vacuum. The binding

energies were internally referenced to C1s peak at 284.6 eV.

Transmission infrared spectra of catalysts were collected in situ in a reactor cell placed in a Bruker vertex 70

Fourier transform infrared (FTIR) spectrometer. The IR cell was equipped with CaF_2 windows, connections for

inlet and outlet flows, and thermocouples to monitor and control the temperature. Before introducing CO, the

samples were reduced in H_2 at 723 K for 3 h, then cooled to room temperature in a He flow and exposed to CO for

3h for saturation. The samples were then purged in an Ar flow for 30 min to remove gaseous and weakly adsorbed

CO species. The spectra were obtained in the absorbance mode and were presented after subtraction of a

background spectrum obtained on the freshly reduced samples.

2.4. Phenol hydrodeoxygenation evaluation

For the hydrodeoxygenation reaction, phenol (0.27 g), dodecane as a solvent, (20 mL) and catalyst (0.1 g)

were firstly loaded into an autoclave (100 mL). This reactor was flushed with N_2 to remove air and then stably

pressurized with H_2 to 2.0 MPa at room temperature. After the autoclave was heated to 453 or 493 K, the reaction

lasted for a certain hour. At last, the liquid product was analyzed with a gas chromatograph (SHIMADZU GC2010)

equipped with an auto-sampler and a flame ionization detector using N_2 as carrier gas. Isooctane was used as the

internal standard for the quantification of products.

3. Results and discussion

3.1. Phenol hydrodeoxygenation and physiochemical characterization over Ni_2P/SiO_2

Figure 1 shows the phenol conversion and product selectivity over at 453 and 493K. With the increasing in

Ni_2P loading, the catalytic activity increases and then decreases at 453 or 493K. The similar change tendency is

also found over Ni_2P/SiO_2 for benzofuran hydrodeoxygenation [15]. Figure S1 demonstrates the XRD patterns of

Ni_2P/SiO_2 with different loadings. There is no prominent Ni_2P diffraction peak at 5%Ni_2P/SiO_2 compared with the

other samples due to low loading and high distribution of Ni_2P. However, excess loading leads to the larger particle

size of Ni_2P and correspondingly decreasing of hydrodeoxygenation activity. The appropriate catalyst is

10%Ni_2P/SiO_2 for phenol hydrodeoxygenation. TEM micrograph in Figure 2 presents the distribution of the Ni_2P

6

particle size on Ni_2P/SiO_2 catalysts. With the increasing in the loading from 5 to 15%, Ni_2P particle size increases

from about 2nm to 6nm. $10\%Ni_2P/SiO_2$ has uniform particle size of 3.2nm. This is similar to XRD result from

scherrer formula.

Cyclohexane, cyclohexanol and cyclohexanone are main products on Ni_2P/SiO_2 at 453K (Figure 1).

Cyclohexanol and cyclohexanone are intermediates for phenol hydrodeoxygenation to cyclohexane [16]. The higher

reaction temperature favors the formation of the more cyclohexane. Thus, cyclohexane selectivity prominently

rises and those of cyclohexanol and cyclohexanone dramatically drop, accompanied by the increasing in phenol

conversion when the reaction temperature increases from 453K to 493K.

3.2. Physiochemical characterization and phenol hydrodeoxygenation of noble metal- Ni_2P/SiO_2

Figure 3 demonstrates catalytic results over noble metal-Ni_2P/SiO_2 catalysts at 453 and 493K. With the

addition of noble metal, the catalytic activities of Ni_2P/SiO_2 increase dramatically. At the same time, the selectivity

of cyclohexanol increases while that of cyclohexanone decreases at 453K. In other words, the existence of noble

metal leads to the generation of a great deal of cyclohexanol with the increasing in the phenol conversions over

noble metal-Ni_2P/SiO_2 catalyst. In comparison with supported noble metal catalysts (Figure S2), the catalytic

activity over noble metal-Ni_2P/SiO_2 changes slightly. However, cyclohexane and cyclohexanol selectivities

increase and cyclohexanone decreases obviously. This is mainly because the existence of Ni_2P intensifies the

deoxygenation and carbonyl hydrogenation over noble metal-Ni_2P/SiO_2.When reaction temperature further

increases up to 493K, the effects of the addition of noble metal on catalytic activities are not prominent, since 10%

Ni_2P/SiO_2 has high phenol conversion, 92.6%, and the rise of catalytic activities is limited. However, the main

products also change from cyclohexanol at 453K to cyclohexane at 493K on noble metal-Ni_2P/SiO_2. Effect of

reaction time on product selectivities (Figure S3) also confirms that cyclohexanol can gradually convert into

cyclohexane with reaction time prolonging over $1\%Pd-10\%Ni_2P/SiO_2$. Thus, in comparison with pure noble metal

or Ni_2P catalysts, synergistic effect of hydrodeoxygenation from Pd and deoxygenation and carbonyl hydrogenation from Ni_2P gives rise to the increment of hydrodeoxygenation activity and differences of selectivity on noble metal-Ni_2P catalysts as well as higher reaction temperature and longer time. In addition, the catalytic activities over supported catalysts were compared with the mixture of $1\%Pd/SiO_2$ and $10\%Ni_2P/SiO_2$[17] (Figure 4 and Table S1). The result showed that $1\%Pd-10\%Ni_2P/SiO_2$ has the higher phenol conversion and cyclohexane selectivity than the pure and physically mixed samples. This implies again the occurrence of synergistic effect between noble metal and Ni_2P on $1\%Pd-10\%Ni_2P/SiO_2$.

Thus, a series of physicochemical characterizations were conducted to further unravel the root of catalytic performances improvement of noble metal-Ni_2P/SiO_2. Table 1 demonstrates the BET surface area, pore volume, pore size and CO chemisorption for different catalysts. As shown in Table 1, compared with support Si_2O, BET surface area and pore volume of the $10\%Ni_2P/SiO_2$ decrease with the addition of phosphorus precursor. This indicates that part of catalyst pores was blocked by phosphorus source during the impregnating process. On the other hand, with the addition of noble metal, pore size and surface area rise for noble metal-Ni_2P/SiO_2. The increment of pore size results from the consumption of part Ni_2P. At the same time, only noble metal precursors contacting with dispersed Ni_2P can convert into noble metal nanoparticle because of Ni_2P reducing precursors of noble metal during the preparation process. As a result, the increasing of surface area is a compromise between the consumption of part Ni_2P and high dispersion of generated noble metal nanoparticle. In addition, with the addition of noble metal, the number of active site also increases, except for $1\%Ru-10\%Ni_2P/SiO_2$. If it is assumed that CO linearly adsorbs on nickel atoms of the Ni_2P, as theoretically and experimentally shown by Nelson et al. [18] and Layman and Bussel [19], respectively, and the same type adsorption on noble metal atoms except for partially bridge one for Pd and Ru, then the more CO chemisorption uptake implies that the more active sites for hydrodeoxygenation are generated with the addition of noble metal. As shown in Table 1, the changes trend for CO

8

chemisorption uptake is $1\%Pd-10\%Ni_2P/SiO_2 > 1\%Pt-10\%Ni_2P/SiO_2 >10\%Ni_2P/SiO_2 \approx1\%$ $Ru-10\%Ni_2P/SiO_2$. This is roughly consistent with the activity result of catalysts. Thus, the high hydrodeoxygenation capacity of $Pd/Pt-Ni_2P/SiO_2$ is partly attributed to the increase of active site.

Figure 5 shows the XRD patterns of noble metal-Ni_2P/SiO_2. XRD diffusion peaks of Ni_2P (111), Pd(111), Pt(111) and Ru(111) are 40.714 (PDF#74-1385),40.365 (PDF#87-0645), 39.796 (PDF#87-0646) and 40.772° (PDF#88-2333), respectively. Diffusion intensity of Ni_2P (111) peak is relatively weak while that of noble metal becomes prominent with the addition of noble metal. This implies that the generation of noble metal nanoparticle is at the expense of Ni_2P. XRD pattern shows that Ni_2P (111) peak shifts towards lower angle, Pd(111), Pt(111) with the addition of noble metal, respectively, except for $Ru-Ni_2P/SiO_2$ with weak diffusion. This result indicates that Pd (0.179nm) or Pt (0.183nm) with the larger atomic radius has doped into Ni_2P (Ni (0.124nm)) or the addition of Pd or Pt leads to lattice distortion of Ni_2P. [20] Furthermore, we believe that an interaction between noble metals and Ni_2P is formed.

HADDF-STEM mapping demonstrates the distributions of palladium, nickel and phosphorus in Figure 6. The loading site of phosphorous precursor is uncontrollable while the formation of Pd depends on Ni_2P reducing. As shown in Figure 6, the distribution density of Pd is mainly consistent with that of Ni_2P. This result further verifies that controllable distribution of noble metal nanoparticle is achieved and the intimate contact structure between noble metal and Ni_2P is formed by Ni_2P reducing noble metal precursor. Combined with CO chemisorption and XRD results, we speculated that controllable distribution of noble metal nanoparticle results in intimate contact between noble metal and Ni_2P, further leading to interaction between both of them and increment of active site, compared with 10% Ni_2P/SiO_2.

Figure 7 shows XPS spectra of different pure noble metal and composite catalysts. It has been noted that the signal to noise ratio is similar for the three couples of samples containing Pd, Pt and Ru, respectively, and that the

intensity differences between SiO_2 supported sample and Ni_2P/SiO_2 supported are in the same direction. This

implies that noble metal-Ni_2P/SiO_2 might have the stronger signal for XPS spectra than pure noble metal catalysts.

In addition, Table S2 also demonstrated the surface atomic ratios with respect to Si, O and noble metal of these

catalysts. Comparison showed also that composite catalysts have the higher loading ratios of noble metal on the

surface than SiO_2 supported catalyst. This result might be related to Ni_2P reducing noble metal precursor into

nanoparticles. Existence of reductant Ni_2P contributes to the generation of the more noble metal particles. On the

other hand, spectrum peak of Pd over 1%Pd-10%Ni_2P/SiO_2 shifts toward the low binding energy compared with

pure noble metal catalysts. The XPS signal of supported metal particles shifts to higher binding energy with the

decreasing in particle size[21]. Meanwhile, the electron transferring from Ni_2P to noble metal renders the latter

electron rich and the corresponding signal toward the lower binding energy. Therefore, Pd spectrum peak shifting

toward the low binding energy in Figure 7 is a compromise result from the smaller noble metal particle and

electron transferring. However, this electron transferring was likely the reason of high catalytic performances on

Pd-Ni_2P/SiO_2. As proposed by Ueckert et al.[22], the metal site with a high electron density favors the formation of

the π back bond between the aromatic ring and metal sites, which promotes the hydrogenation of the aromatic ring.

Moreover, since the lowest unoccupied molecular orbital (LUMO) of C-O is antibonding and surfaces that are able

to transfer electron density to this orbital facilitate the dissociation of the C-O bond [23], the increased electron

density of Pd accounts for the higher hydrodeoxygenation catalytic activity on Pd-Ni_2P/SiO_2. For product

selectivity, cyclohexanol increases while cyclohexanone decreases on noble metal-Ni_2P/SiO_2 catalysts due to

improvement of hydrogenation capacity in comparison with 10%Ni_2P/SiO_2 at 453K. As mentioned above,

synergistic effect of hydrodeoxygenation from Pd and deoxygenation and carbonyl hydrogenation from Ni_2P

results in the promotion of catalytic performances on noble metal-Ni_2P catalysts. Herein, this effect is mainly due

to the interaction between Ni_2P and noble metal and electron transfer from Ni_2P to Pd on Pd-Ni_2P/SiO_2. As

reaction temperature rises from 453K to 493K, the main product changes from cyclohexanol to cyclohexane

because of intensifying of deoxygenation at higher temperature. In contrast, although electron also transfers from

Ni_2P to Pt on noble metal-Ni_2P catalysts [11], 1%Pt-10%Ni_2P/SiO_2 exhibits the lower catalytic selectivity as well as

the higher conversion than Ni_2P/SiO_2. That is, the synergistic effect of Pt and Ni_2P on catalytic performances is

less prominent than Pd-Ni_2P/SiO_2. Ru exists in the form of Ru^{4+} in 1% Ru-10% Ni_2P /SiO_2 because Ru is prone to

oxidation again. Ru oxidized and less active site on 1%Ru-10% Ni_2P/SiO_2 account for the lower the catalytic

performance than other composite catalysts.

The element electronegativity represents the capability of atom drawing electron. The larger

electronegativity means that this atom has the greater ability to withdraw electron. For Ni_2P, $Ni^{\delta+}$ ($0 < \delta < 2$)

covalently bonds with $P^{\delta-}$ ($0 < \delta < 1$). Ni has the smaller electronegativity (1.91) while that for phosphorus is 2.19.

There is a small electron transfer from Ni to P in nickel phosphide. In contrast, the electronegativity of Pd, Pt and

Ru is 2.20, 2.28 and 2.20, respectively. Noble metal contacting with Ni_2P probably accepts electrons from nickel

due to the larger electronegativity of noble metal.

CO-FTIR spectroscopy was also performed to further verify the electronic contribution on supported

catalysts (Figure 8). FTIR spectra of adsorbed CO shifts from 2077 cm^{-1} to the higher wavenumber, 2094, 2083

and 2079 cm^{-1}, respectively, with the Pd, Pt and Ru addition. According to the Blyholder model [24], this shift toward

higher frequencies is indicative of the strengthening of the CO bond due to decreased d-electron of metal into the

CO π^* antibonding orbital by back-electron transferring [25]. Since the presence of Pd gives rise to electron donation

from Ni_2P to Pd, the electron enrichment on Pd and electron deficiency on Ni_2P occur, as also reported by the XPS

data. Thus, metal d-electron transferring into the CO π^* antibonding orbital decreases and stretching vibration of

CO adsorbed shifts toward higher frequencies.

In addition, the vibration frequency of CO adsorbed on catalysts between 2077 and 2094 cm^{-1} also indicates

that most of CO is linearly adsorbed on noble metal-Ni$_2$P/SiO$_2$ in agreement with the assumption for the

determination of active sites in CO chemisorption. However, we also notice that the intensity change of the CO

stretching vibration with the addition of noble metal is not consistent with the active site number by CO

chemisorption. Utilizing CO-FTIR for quantification is inaccurate due to the effects of the loading of catalysts and

roughness of tested surface. In comparison with CO-FTIR, CO chemisorption is a typical method to determine the

active site of catalysts. Therefore, herein CO-FTIR is performed to only confirm the electron transferring from

Ni$_2$P to noble metal on catalyst surface.

Evaluation and characterization results suggested that the key factors influencing the catalyst activity and the

selectivities to different products were the more active sites and the electron transfer from Ni$_2$P to Pd with the

addition of noble metal as well as appropriate reaction temperature and time. Further, the increment of active sites

and the electron transfer are from the reduction of noble metal precursor on Ni$_2$P/SiO$_2$ and the interaction between

Ni$_2$P and noble metal. Based on experimental results, a possible deoxygenation scheme over noble

metal-Ni$_2$P/SiO$_2$ is also suggested as follows (Figure 9). Pure Ni$_2$P has the higher selectivity to cyclohexanone and

cyclohexanol. In contrast, cyclohexanone can continue to hydrogenate into cyclohexanol over noble

metal-Ni$_2$P/SiO$_2$ under the same reaction conditions due to synergistic effect of Ni$_2$P and Pd. When reaction

temperature further increases or hydrodeoxygenation time prolongs, cyclohexanol can continue to convert into

cyclohexane over noble metal-Ni$_2$P/SiO$_2$. In terms of Ni$_2$P catalyst system, benzene, however, is generated rarely.

4. Conclusions

10%Ni$_2$P/SiO$_2$ prepared from the sol-gel and TPR method has the uniform distribution of Ni$_2$P

nanoparticle and relatively high active activity for phenol hydrodeoxygenation. With the addition of noble

metal, especially for Pd, noble metal-Ni$_2$P/SiO$_2$ catalysts generate more cyclohexanol, compared with pure

Ni$_2$P or noble metal supported catalysts at 453K. When reaction temperature further rises, the main

products also change from cyclohexanol at 453K to cyclohexane at 493K on Ni$_2$P/SiO$_2$ or noble

metal-Ni$_2$P/SiO$_2$. In addition, 1%Pd-10Ni$_2$P/SiO$_2$ presents the higher catalytic performances than

supported or physically mixed catalysts. As for noble metal and Ni$_2$P composite catalyst, controllable

distribution of noble metal and intimate contact between Ni$_2$P and noble metal result in interaction

between both of them and facilitate the increasing in active site and electron transferring from Ni$_2$P to

noble metal. Synergistic effect of deoxygenation and carbonyl hydrogenation from Ni$_2$P and

hydrodeoxygenation from Pd gives rise to the increment of hydrodeoxygenation activity and the

generation of a large amount of cyclohexanol at 453 K and cyclohexane product at 493 K.

Acknowledgements

References

1   H. Xu, K. Wang, H. Zhang, L. Hao, J. Xu and Z. Liu, *Catal. Sci. Technol.,* 2014, **4**, 2658.

2   D. A. Ruddy, J. A. Schaidle, J. R. Ferrell III, J. Wang, L. Moens and J. E. Hensley, *Green Chem.,* 2014, **16**, 454.

3   H. Wang, J. Male and Y. Wang, *ACS Catal.,* 2013, **3** ,1047.

4   J. Moon, E.-G. Kim and Y. K. Lee, *J. Catal.,* 2014, **311**, 144.

5   E. Muthuswamy, G.H.L. Savithra and S.L. Brock, *ACS Nano*, 2011, **5**, 2402.

6   Q. Guan and W. Li, *J. Catal.*, 2010,**271**, 413.

7   J. Chen, Y. Chen, Q. Yang, K. Li and C.Yao, *Catal. Commun.*, 2010,**11**,571.

8   M. Á. González-Borja and D.E. Resasco, *Energy Fuels,* 2011, **25**, 4155.

9   J. Sun, A.M. Karim, H. Zhang, L. Kovarik, X.S. Li, A.J. Hensley, J.-S. McEwen and Y Wang. *J. Catal.,* 2013, **306**,47.

10   N. Yan, Y. Yuan, R. Dykeman, Y. Kou and P.J. Dyson, *Angew. Chem. Int. Ed.,* 2010, **49**, 5549.

11   Y.-K. Hong, D.-W. Lee, H.-J. Eom and K.-Y. Lee, *Appl. Catal. B.,* 2014, **150-151**,438.

12   J. Chang, L. Feng, C. Liu, W. Xing and X. Hu, *Angew. Chem. Int. Ed.,* 2014, **53**, 122.

13   J. Chang, L. Feng, C. Liu, W. Xing and X. Hu, *Energy Environ. Sci.,* 2014, **7**, 1628.

14   V. T. Silva, L. A. Sousa, R. M. Amorim, L. Andrini, S.J.A. Figueroa, F. G. Requejo and F.C. Vicentini, *J. Catal.,* 2011, **279**, 88.

15   B. Güvenatam, O. Kurşuna, E. H. J. Heeres, E. A. Pidko and E. J. M. Hensen, *Catal. Today*, 2014, **233**, 83.

16   S. T. Oyama, X. Wang, Y.-K. Lee and W.-J. Chun, *J. Catal.,* 2004, **221**, 263.

17.   R.X. Liu and F.Y. Zhao, *SCI. CHINA Chem.* 2010,**53 (7)**: 1571

18.   A. E. Nelson, M. Sun and A. S. M. Junaid *J. Catal.,* 2006, **241**, 180.

19..   K. A. Layman and M. E. Bussell, *J. Phys. Chem. B.,* 2004,**108**, 15791.

20.   R. Jing, S.X. Liang, C.Y. Liu, M.Z. Ma, X.Y. Zhang and R.P. Li, *Mater. Sci. Eng. A.*, 2012, **552**, 295

21.   W. P. Zhou, A. Lewera, R. Larsen, R. I. Masel, P. S. Bagus, and A. Wieckowski, *J. Phys. Chem. B.,* 2006, **110**, 13393

22.   T. Ueckert, R Lamber, N. I. Jaeger and U. Schubert, *Appl. Catal. A.,* 1997, **155 (1)**, 75.

23.   V. M. L. Whiffen and K .J. Smith, *Energy Fuels*., 2010,**24**, 4728.

24.   G. Blyholder. *J Chem Phys.*, 1964, **68**, 2772.

25.   H. Zhao, S. T. Oyama, H.-J. Freund, R. Włodarczyk and M. Sierka, *Appl. Catal. B.*, 2015,**164**, 204.

15

Table legends

Table 1. Textural and structural properties of different catalysts

Table 1

Catalyst	Pore size(nm)	Pore volume (cm^3/g)	BET Surface Area (m^2/g)	CO uptake(umol/g)
SiO_2-sol-gel	9.30	0.98	421.00	--
$10\%Ni_2P/SiO_2$	10.03	0.90	238.55	92.25
$1\%Pt-10\%Ni_2P/SiO_2$	11.60	0.85	293.63	109.51
$1\%Ru-10\%Ni_2P/SiO_2$	11.49	0.88	307.39	90.77
$1\%Pd-10\%Ni_2P/SiO_2$	15.62	1.00	257.12	121.32

Figure captions

Figure 1 Phenol conversion and product selectivities over the different Ni_2P/SiO_2 catalysts: a, b 453K; c, d 493K.

Figure 2 TEM images and particle size distribution for the different Ni_2P/SiO_2 catalysts: a.5%, b.10% and c.15%.

Figure 3 Phenol conversion and product selectivities over the different noble metal-Ni_2P/SiO_2 catalysts: a, b 453K; c, d 493K

Figure 4 Phenol conversion and product selectivities over 1%Pd-10%Ni_2P/SiO_2 and the physical mixture of Pd/SiO_2 and Ni_2P/SiO_2

Figure 5 XRD diffraction patterns of the different noble metal-Ni_2P/SiO_2 catalysts

Figure 6 HADDF-STEM of 1.0%Pd-10%Ni_2P/SiO_2

Figure 7 XPS spectra of different noble metal-Ni_2P/SiO_2 catalysts

Figure 8 Infrared spectra of adsorbed CO on 10%Ni_2P/SiO_2, 1%Pd-10%Ni_2P/SiO_2, 1%Pt-10%Ni_2P/SiO_2 and 1%Ru-10%Ni_2P/SiO_2

Figure 9 A possible deoxygenation scheme for noble metal-Ni_2P/SiO_2
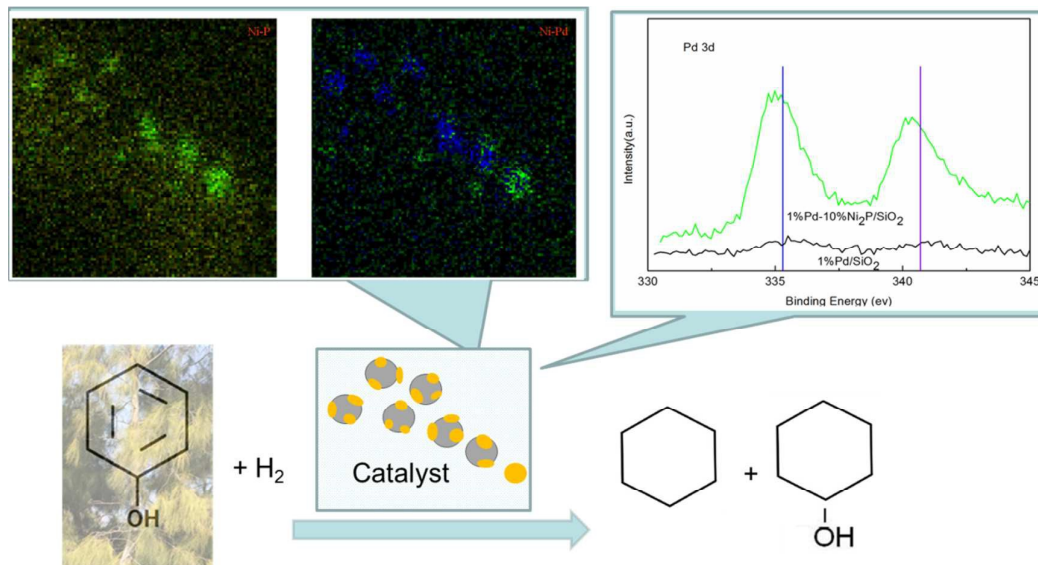
1%Pd-10%Ni$_2$P/SiO$_2$ from Ni$_2$P reducing noble metal precursor presents the high activity and cyclohexanol or cyclohexane selectivity due to the more active site and electron transferring from Ni$_2$P to noble metal.
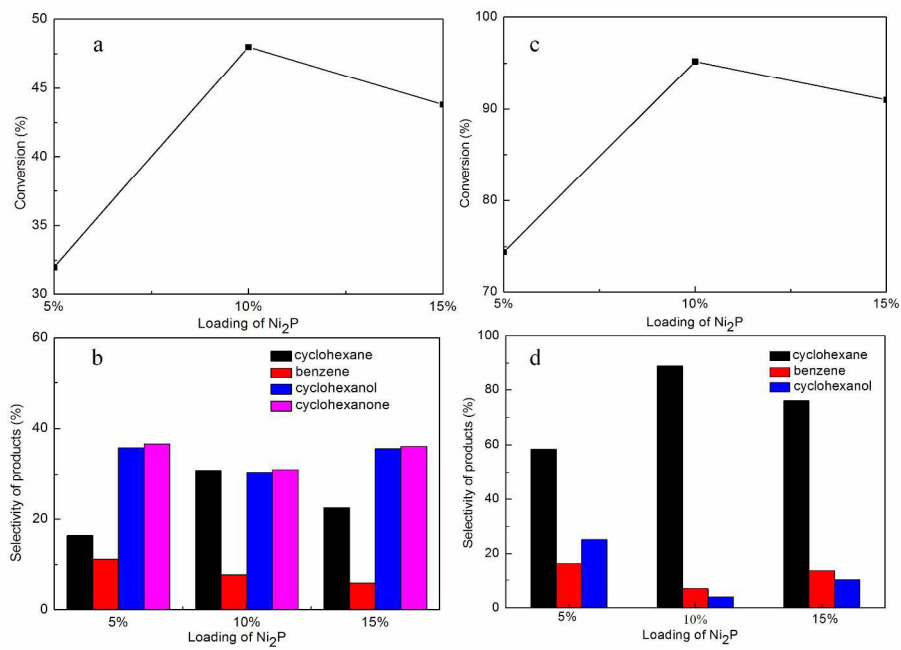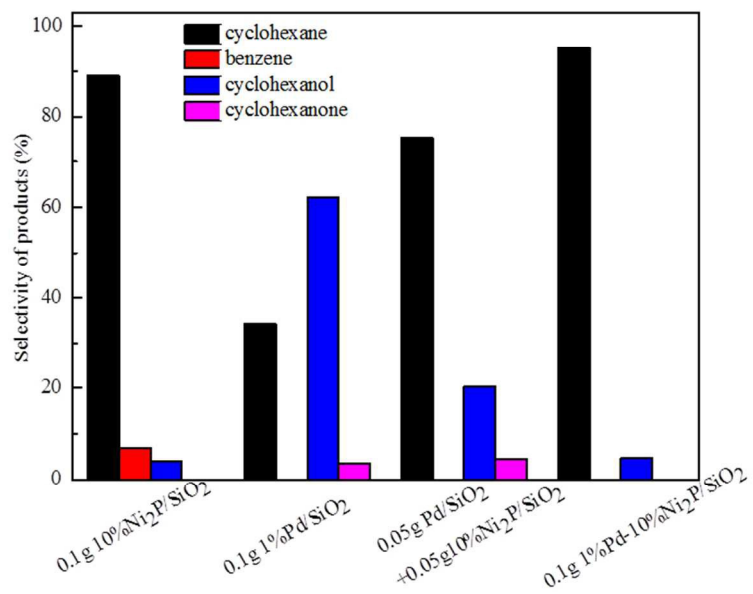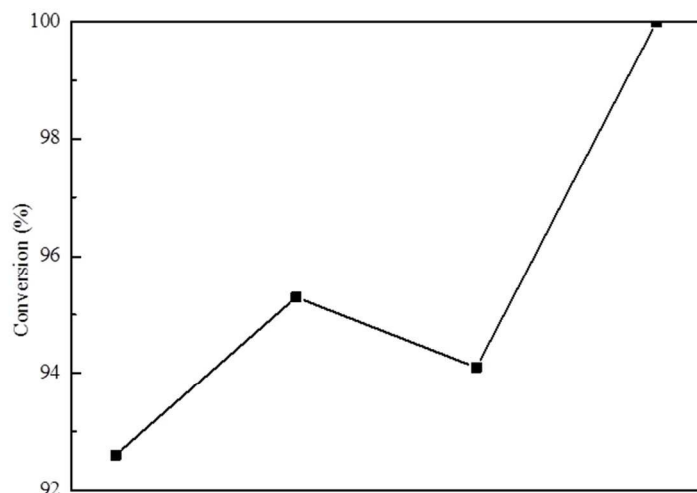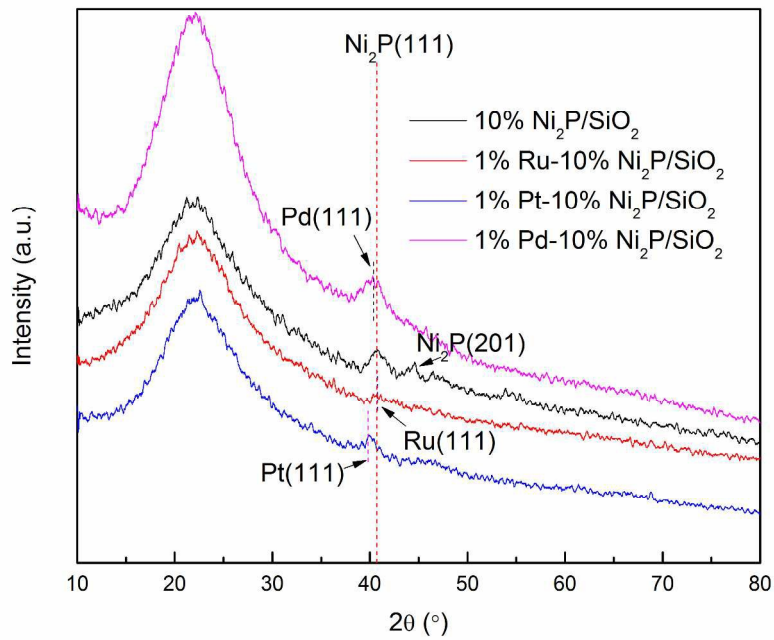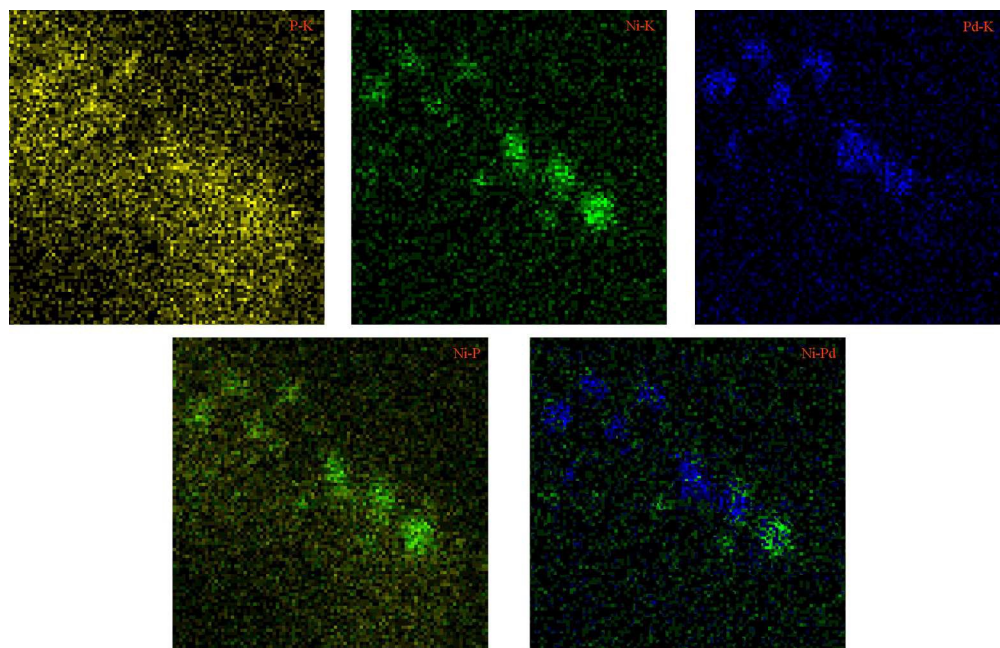
289x203mm (300 x 300 DPI)
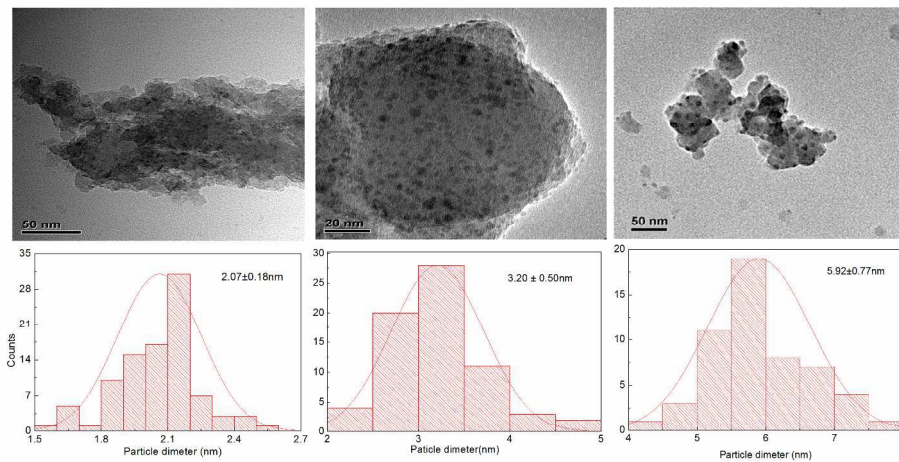
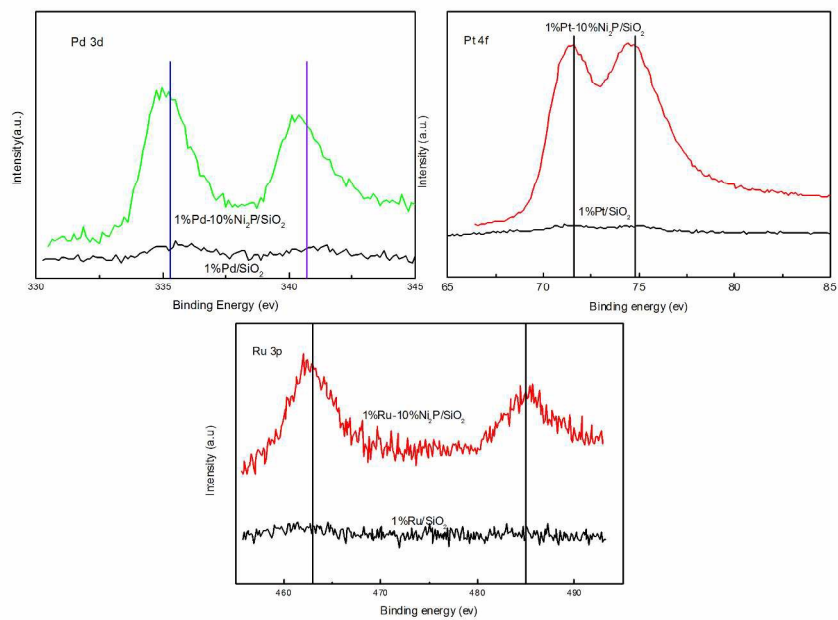289x203mm (300 x 300 DPI)
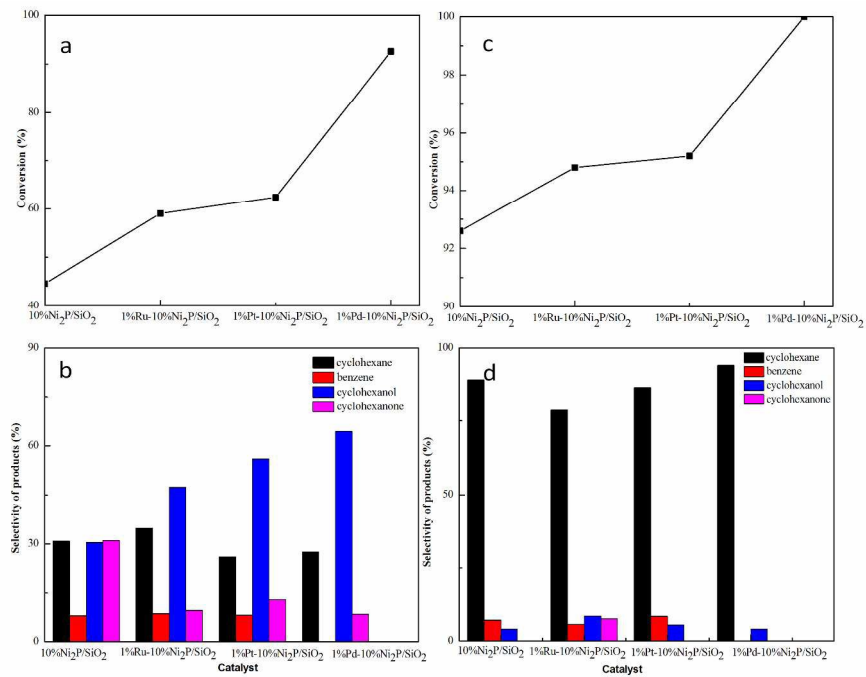
289x203mm (300 x 300 DPI)
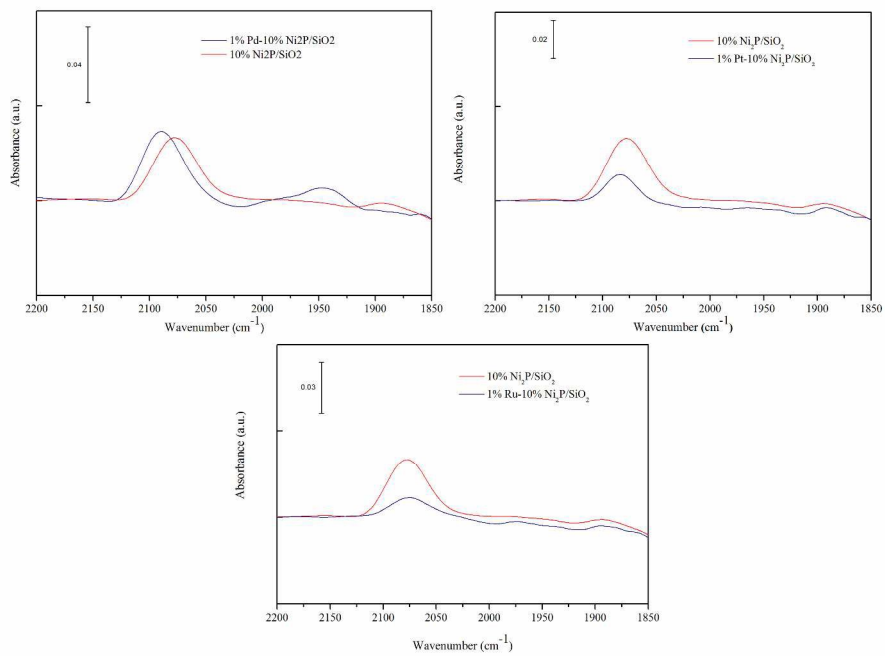
144x186mm (150 x 150 DPI)
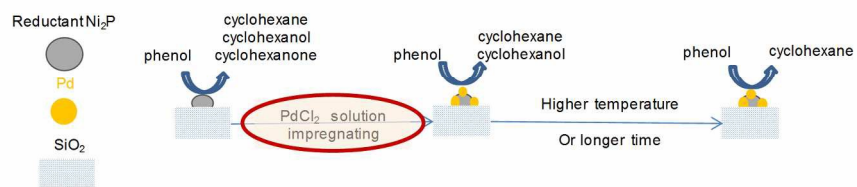
279x215mm (300 x 300 DPI)

729x480mm (72 x 72 DPI)

289x203mm (300 x 300 DPI)

288x201mm (300 x 300 DPI)

177x50mm (300 x 300 DPI)